

# Progressive seismic failure of a highway bridge, including abutment–backfill interaction

Mouloud Ouanani and Boualem Tiliouine\*

Ecole Nationale Polytechnique, Civil Engineering Department, Laboratory of Earthquake Engineering and Structural Dynamics, Avenue H. Badi, El Harrach, 16200 Algiers, Algeria

**Current engineering practice pays little attention, if any, to nonlinear abutment–backfill soil interaction (ABSI) effects on seismic behaviour of bridges. The primary focus of this article is to assess the influence of ABSI on the progressive seismic failure of bridge structures. Emphasis is placed on the significance of ABSI effects, including abutment behaviour and backfill soil flexibility. Nonlinear dynamic analysis is performed using a bilinear hysteretic model for the bridge superstructure and nonlinear characteristics of the expansion joint. Results indicate that ABSI has a significant effect on the seismic response in the longitudinal direction and can effectively reduce bridge seismic demands. ABSI affects rotational ductility demand at pier ends of the bridges, relative displacements, pounding and axial forces in the restrainers. Thus, it is essential that numerical models used in seismic assessment of bridge structures properly consider abutment–backfill interaction.**

**Keywords:** Abutment–backfill soil interaction, highway bridges, nonlinear dynamic analysis, seismic failure.

HIGHWAY bridges represent structures of economic and strategic importance. They are generally built in reinforced or prestressed concrete to span over a valley, river, road or any physical obstacle to essentially allow the passage of all kinds of vehicles. High seismic performance is usually required for this special category of structures, the potential collapse of which can result in a significant economic impact.

Abutment modelling and behaviour<sup>1</sup>, soil conditions and foundation soil stiffness<sup>2</sup>, soil structure interaction<sup>3</sup> and embankment flexibility<sup>4</sup> have been found to significantly influence the response of bridge systems and eventually their seismic failure<sup>5</sup> under strong ground motions. In addition, analysis of past and recent bridge damage data has illustrated that seismic participation of bridge abutment and backfill soil can lead to cost-effective design of bridges<sup>6</sup>.

The primary focus of this article is to assess the influence of abutment–backfill soil interaction (ABSI) on the

progressive seismic failure of bridge structures. Emphasis is placed on the significance of ABSI effects, including abutment behaviour and flexibility of backfill soil at the abutments. The effective stiffness, foundation soil damping and capacity parameters at the base of the spread footings have been evaluated using FEMA procedures<sup>7</sup>. Yields strengths of abutment backfill in compression and in tension have been evaluated using Mononobe–Okabe pseudostatic approach for passive force and frictional sliding capacity at the abutment footing respectively. Nonlinear dynamic analysis is performed using a bilinear hysteretic model for the bridge superstructure and nonlinear characteristics of the expansion joint. Based on the results obtained in the present study, it is concluded that ABSI has significant influence on seismic demands of bridge systems and hence can lead to cost-effective design of bridge structures. However, special attention should be given to axial forces in the restrainers whose displacements can be, under certain design conditions, increased due to yielding of backfill soil.

## Description of highway bridge

The reinforced concrete bridge structure considered in this study is a typical long-span box girder bridge with expansion joints and elastomeric bearings at the abutments. This highway bridge is of strategic importance and is to be built in order to connect Mascara downtown and Hallilef faubourg in Algeria. This bridge is situated in Mascara district, NW Algeria, classified under seismic zone IIa with an expected  $PGA = 2.697 \text{ m/s}^2$ , in accordance with the Algerian seismic design code<sup>8</sup>. Figure 1 *a–d* presents the cross-section of segments and piers and seat-type abutment of the actual bridge.

Young's modulus of concrete is 33 GPa for all piers and abutments, while it is taken as 36 GPa for the bridge deck. Mass density of concrete is estimated to be equal to  $2500 \text{ kg/m}^3$ . A constant 5% damping value is taken for both the first and second vibration modes in order to estimate the damping matrix of the bridge system.

The actual site conditions are of  $S_D$  type (i.e. high stiff soil profile with initial shear wave velocity  $V_s = 366 \text{ m/s}$ ). The weight density and Poisson ratio are:  $\gamma = 21 \text{ KN/m}^3$  and  $\nu = 0.40$  respectively.

\*For correspondence. (e-mail: boualem.tiliouine@g.enp.edu.dz)

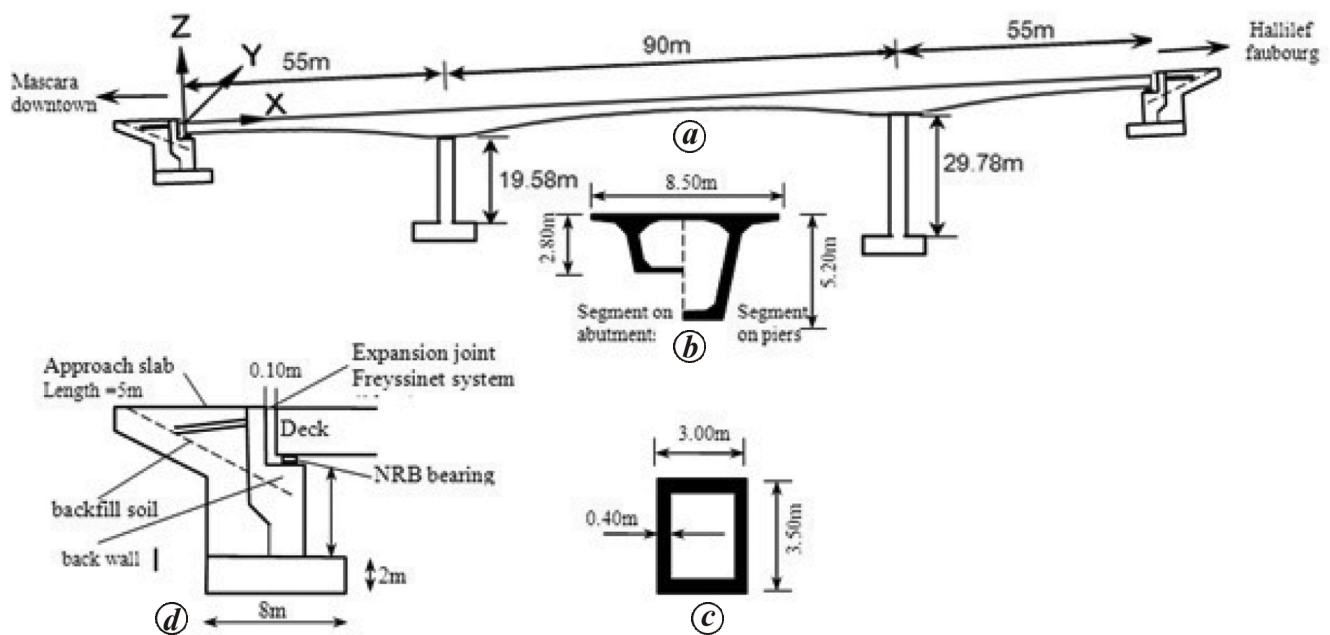


Figure 1. Description of bridge: (a) Elevation of bridge, (b) cross-section of segments, (c) cross-section of pier and (d) seat-type abutment.

**Soil stiffness and damping matrices**

The elements of foundation soil stiffness and damping matrices have been evaluated using the analytical expressions derived from theoretical solutions of a circular footing bonded to the surface of an elastic half space<sup>9</sup>

$$K_x = \frac{8G}{2-\nu} R_x; K_z = \frac{4G}{1-\nu} R_z; K_{\theta_y} = \frac{8G}{3(1-\nu)} R_{\theta_y}^3, \tag{1}$$

$$C_x = \frac{4.6G}{(2-\nu)V'_S} R_x^2; C_z = \frac{3G}{(1-\nu)V'_S} R_z^2; \text{ and}$$

$$C_{\theta_y} = \frac{0.4G}{(1-\nu)V'_S} R_{\theta_y}^4. \tag{2}$$

The coefficients ( $K_x, C_x$ ) and ( $K_z, C_z$ ) on the one hand, and ( $K_{\theta_y}, C_{\theta_y}$ ) on the other, are translational and rotational stiffnesses and dashpot coefficients respectively, associated with  $x$  and  $z$  directions.  $\nu$  is the Poisson ratio coefficient whereas  $G$  and  $V'_S$  are respectively, the effective shear modulus and effective shear wave velocity consistent with the type of soil and PGA design value. The extra-diagonal terms of the  $3 \times 3$  foundation soil stiffness and damping matrices may be calculated using the following expressions

$$K_{x\theta_y} = \frac{0.56G}{(2-\nu)} R_{\theta_y}^2; C_{x\theta_y} = \frac{0.4G}{(2-\nu)V'_S} R_{\theta_y}^3. \tag{3}$$

For a rectangular foundation, the radii  $R_x, R_z$  and  $R_{\theta_y}$  for the equivalent circular foundation and the associated

attached soil masses have been evaluated using FEMA procedures<sup>7,9</sup>.

**Abutment wall stiffness**

Full-scale bridge abutment passive earth pressure experimentation and simulation have shown that soil structure interaction (SSI) and backfill soil flexibility can significantly influence the earthquake response of bridge structures<sup>1</sup>.

In this study, design procedures and guidelines are utilized to evaluate back wall translational and rotational stiffnesses<sup>10</sup>.

In Figure 2, the resultant back wall longitudinal translational ( $K_w$ ) and rotational ( $K_{rw}$ ) stiffnesses act at a distance  $h_1 = 0.37 H_w$  from the bottom tip of the abutment (Figure 2 a) and can be obtained using the following equations<sup>10,11</sup>

$$K_w = 0.425 E_s B_w; K_{rw} = 0.072 E_s B_w H_w^2, \tag{4}$$

where  $E_s$  is the backfill soil Young's modulus and  $B_w$  and  $H_w$  are the width and height of the abutment wall respectively.

*Equivalent foundation springs*

Figure 2 a shows equivalent foundation springs for wing wall and back wall footings as well as the resultant translational and rotational stiffnesses of the back wall.

Based on the assumption of abutment rigid body movement, the translational and rotational stiffness springs

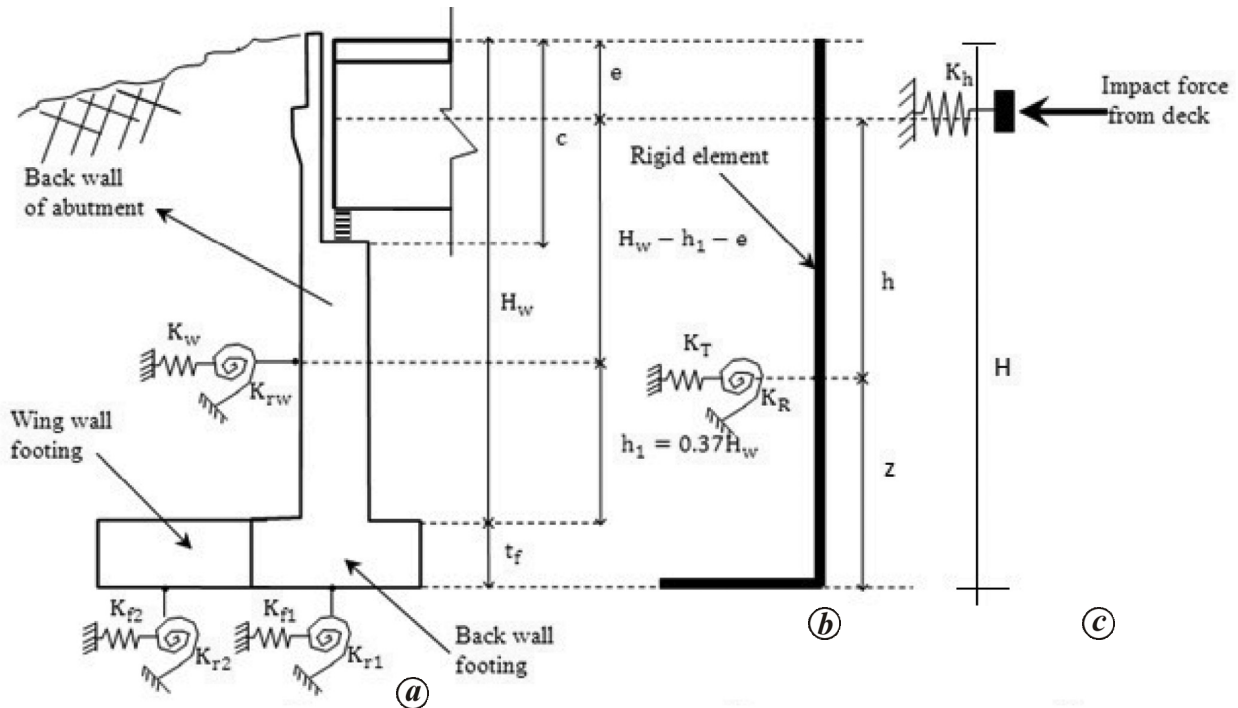


Figure 2. Abutment foundation springs: (a) springs for various components; (b) equivalent springs at the point of impact and (c) simplified model.

indicated in Figure 2 b for both back wall and wing wall footings, as well as for abutment back wall can be transferred to the stiffness centre located at height  $z$  above the footing base.

The resultant translational stiffness can be simply calculated as

$$K_T = K_w + K_{f1} + K_{f2}, \tag{5}$$

where  $K_w$ ,  $K_{f1}$  and  $K_{f2}$  are respectively, the translational stiffnesses of the back wall, and the two wing wall and back wall footings.

The resultant rotational stiffness is

$$K_R = K_{rw} + K_{r1} + K_{r2} + K_w (0.37H_w + t_f - x)^2 + (K_{f1} + K_{f2}) x^2, \tag{6}$$

where  $K_{rw}$  is the back wall stiffness,  $K_{r1}$  and  $K_{r2}$  are the rotational stiffnesses of the back wall foundation and wing wall footings respectively (see Figure 2 a), while  $H_w$  and  $t_f$  are the back wall height and footing depth respectively.

Assuming abutment rigid body movement, it can be shown that the stiffness centre is located at a height  $z$  above the footing base such that

$$z = (0.37H_w + t_f) \frac{K_w}{K_T}. \tag{7}$$

Further, the translational and rotational stiffnesses (Figure 2 b) can be moved to the point of impact supposed to be located at the centroid of the bridge deck, as illustrated in Figure 2 c in the final simplified model.

The equivalent translational stiffness of this simplified spring mass system,  $K_h$ , can be easily calculated from

$$K_h = \frac{K_R K_T}{(K_T h^2 + K_R)}, \tag{8}$$

### Abutment strength

A bilinear load–deformation spring model in bridge longitudinal direction is used to simulate the behaviour of abutment–backfill soil system. The compressive yield strength,  $C_x$ , at the abutments is determined using Mononobe–Okabe approach for passive force as

$$C_x = \frac{1}{2} \gamma H^2 (1 - a_v) K_{PE} B_w, \tag{9}$$

where  $\gamma$  and  $H$  are the unit weight and height of backfill soil respectively.  $B_w$  the abutment width,  $a_v$  the vertical acceleration coefficient and  $K_{PE}$  denotes the earth pressure coefficient determined from the equation

$$K_{PE} = \frac{\cos^2(\varphi - \psi + \theta_v)}{\cos(\psi) \cos^2(\theta_v) \cos(\psi - \theta_v + \delta)} \times \left[ 1 - \sqrt{\frac{\sin(\varphi + \delta) \sin(\varphi - \psi + \beta)}{\cos(\beta - \theta_v) \cos(\psi - \theta_v + \delta)}} \right]^{-2} \tag{10}$$

where  $\varphi$  is the angle of the friction of the soil,  $\theta_v$  the inclination of the wall with respect to vertical,  $\delta$  the soil–wall interface friction angle assumed to be equal to  $\varphi/2$ ,  $\beta$  the

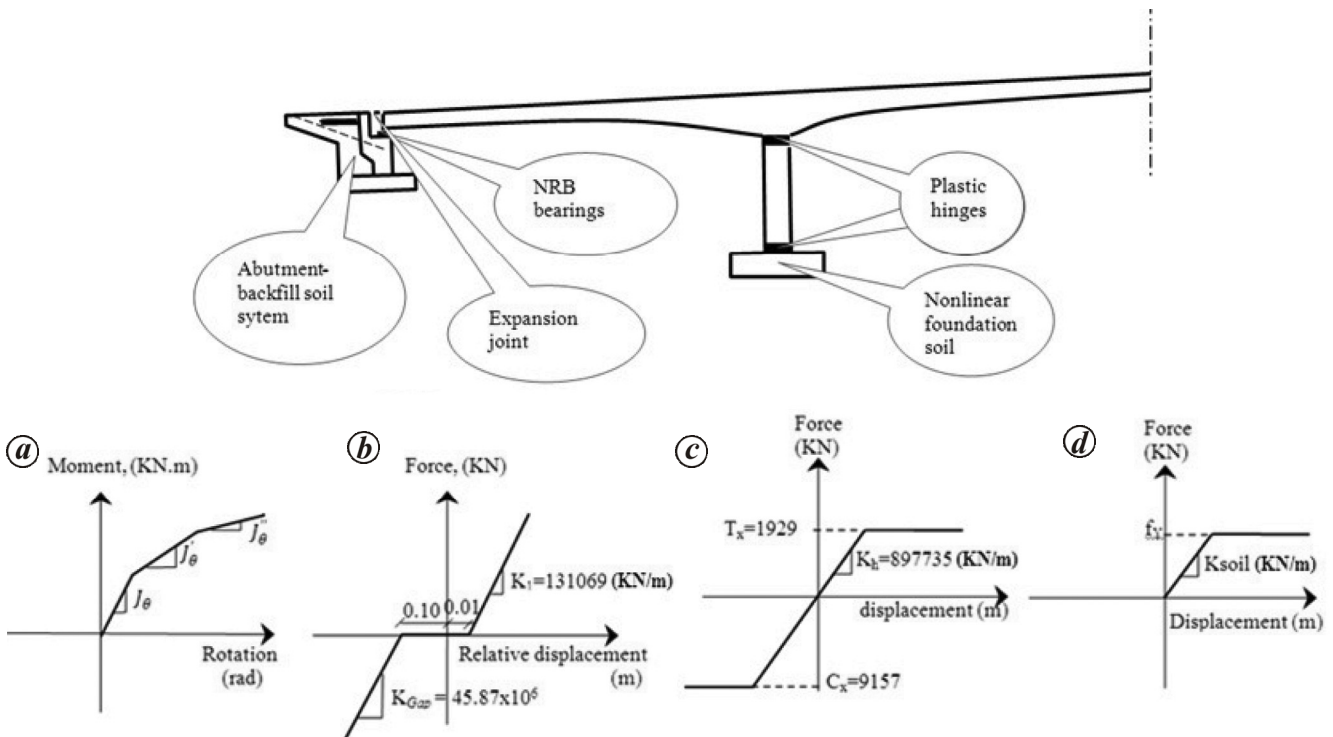


**Figure 3.** Nonlinear model properties of bridge piers, expansion joints, abutment-backfill soil system and foundation soil. *a*, Plastic hinge, including SSI; *b*, expansion joint; *c*, bilinear spring at abutment; *d*, nonlinear foundation soil model.

slope angle of the ground surface and  $\psi$  denotes the seismic inertia angle calculated from the equation

$$\psi = \arctan\left(\frac{a_h}{1 - a_v}\right), \tag{11}$$

where  $a_h$  and  $a_v$  represent the horizontal and vertical acceleration coefficients respectively.

The abutment yield strength,  $T_x$ , under tensile load is supposed to be equal to the frictional sliding capacity, as

$$T_x = N \tan \delta, \tag{12}$$

where  $\delta$  is the frictional angle at the interface of foundation soil–abutment footing and  $N$  is the total force at the interface.

Figure 3 *c* shows the nonlinear load–displacement relationship used to characterize the behaviour of the ABSI system.

### Nonlinear analytical model

The bridge has seat-type flexible abutments in the longitudinal direction, which allow limited longitudinal movement of the superstructure due to the gap between the superstructure and the abutment back wall. The support provided by the abutment is assumed to be fixed

against translation in the vertical direction, translation free in the longitudinal direction and rotational free about the lateral direction.

Seismic excitation of the bridge generates bending moments in piers resulting eventually in plastic hinges at the piers ends. The nonlinear moment–curvature relationships at these plastic hinges have been developed in accordance with the methodology established in Yoshida<sup>12</sup>. Nevertheless, for the sake of convenience, bilinear rotational springs have been used herein to simulate the behaviour of these possible plastic hinges (as shown in Figure 3 *a*). All nonlinearities, including expansion joints involved in the model are also shown in the figure. Hook and gap elements (Figure 3 *b*) are used to simulate the opening and closure of expansion joints respectively. The hook element controls the relative displacement between superstructure and abutment back wall, while the gap element controls pounding effects between superstructure and abutment back wall. The hook and gap elements are modelled by linear springs with stiffnesses being  $K_{restrainer} = 0.13 \times 10^6$  KN/m and  $K_{gap} = 45.87 \times 10^6$  KN/m respectively. The initial slack in restraining cables and the initial gap at expansion joints are taken to be 0.01 and 0.10 m respectively.

Bilinear springs with parameters evaluated in accordance with the procedure described earlier in the text are introduced at the abutments to model ABSI system (Figure 3 *c*).

An elastoplastic soil model is utilized to evaluate the nonlinear seismic response of the coupled foundation

soil–bridge system. Typical parameters of load–displacement characteristics utilized for the elastic–plastic soil model are defined in Figure 3 *d*, where  $K_{\text{soil}}$  represents elastic stiffness and  $f_y$  the capacity parameter for rigid footing subject to vertical, longitudinal loads and moments.

Three-dimensional finite element (FE) modelling of soil idealized as a continuum with solid elements could have been used. However, this would require a pertinent soil constitutive model and an experimental characterization of model parameters. Further, the FE model for continuum soil modelling is complex compared to nonlinear springs modelling, which has the important advantages of simplicity in FE modelling, short CPU time, only few material parameters to be determined, simple connection of the springs to the study structure and the possibility to incorporate cyclic loading effects<sup>2</sup>.

The expected vertical capacity  $Q_c$ , the ultimate moment capacity  $M_c$  and the base traction strength  $V$ , have been evaluated using FEMA procedures<sup>7</sup> and are reported in Table 1. The equivalent translational stiffnesses at each abutment of the bridge with and without backfill are given in the table.

To further evaluate the effects of nonlinear foundation soil stiffness on the overall seismic response of the study bridge, the effective stiffness constants are determined using a simulated acceleration input time history compatible with RPOA<sup>8</sup> spectrum scaled for an expected PGA = 0.70 *g* that represents approximately a probability of exceedance equal to 10% in 50 years. Accordingly, the PGA consistent reduction factors for the effective shear modulus and shear wave velocity obtained using FEMA procedures are calculated to be equal to  $G/G_0 = 0.24$  and  $V_s'/V_s = 0.65$  for the range of average shear strains ( $7.37 \times 10^{-4}$ – $6.17 \times 10^{-3}$ ) interpolated from tabulated values given in Yoshida<sup>12</sup>.

Figure 4 shows the entire bridge system modelled as a lumped mass structure represented by 2DFE model.

**Table 1.** Effective stiffness of foundation soil ( $k$ ), capacity parameters for foundation soil ( $f_y$ ) and equivalent stiffness with and without backfill soil ( $K_h$ )

Soil class $S_D$ (high stiff soil): $G/G_0 = 0.24$ , $V_s'/V_s = 0.65$ for the range of average soil shear strains ( $7.37 \times 10^{-4}$ – $6.17 \times 10^{-3}$ ) expected from 0.7 <i>g</i> EPA event		
$K_{\text{soil}}$	$K_x$ (KN/m)	3,417,561
	$K_z$ (KN/m)	3,579,583
	$K_{\theta_y}$ (KNm/rd)	119,364,909
$f_y$	$Q_c$ (KN)	37,078
	$M_c$ (KN m)	37,999
	$V$ (KN)	11,977
$K_h$	With backfill (KN/m)	897,735
	Without backfill (KN/m)	640,802

### Rotational ductility assessment and the corresponding damage state limits in flexibly-supported structures

To analyse the moment–curvature behaviour in concrete piers, the standard procedure incorporated in the SAP2000 platform has been used<sup>13</sup>.

Plastic hinges have been modelled utilizing bilinear hysteretic spring elements. Following Priestley *et al.*<sup>14</sup>, the load–deformation characteristics of these bilinear elements can be calculated from moment–curvature relationships. The resulting moment–rotation characteristics at the yield and ultimate levels have been determined at each plastic hinge location for each bridge pier in longitudinal direction ( $(M_y, \theta_y)$  and  $(M_u, \theta_u)$  respectively).

#### Global rotational ductility assessment of bridge piers in flexibly-supported structures

To assess the effect of soil flexibility on the inelastic response of bridges, a simple structural idealization is utilized (Figure 5).

For the flexibly-supported system, the rotational ductility of the bridge has been established in the general form<sup>15</sup>

$$\mu_{\theta} = \frac{\theta_f + \theta_y + \theta_p}{\theta_f + \theta_y}, \quad (13)$$

where  $\theta_f$  is the foundation rotation,  $\theta_y$  the rotation at yield of pier caused by bending and  $\theta_p$  is the post-yield rotation.

By combining the flexibility of the nonlinear inelastic spring at base of pier and the linear rotational foundation spring, the final rotational spring can be obtained. As shown in Figure 3 *a*, the corresponding moment–rotation diagram is characterized by a first branch (uncoupled rotational) stiffness equal to  $J_{\theta}$ , a second branch stiffness equal to  $J'_{\theta}$  and a third branch stiffness equal to  $J''_{\theta}$ . These terms have been evaluated using the procedures described in the literature<sup>15,16</sup>.

#### Damage state-based rotational ductility limits of piers, including soil flexibly

The quantified damage state for the bridge piers with rotational ductility limits associated with five damage states ranging from yield to collapse have been established. Following the methodology proposed by Dutta and Mander<sup>17</sup>, five different damage states may be determined based on the yield and ultimate rotations obtained from typical moment–rotation plot shown in Figure 3 *a*. Rotational ductility limits at damage states other than ‘almost none’ and ‘collapse’ of the highway bridge are determined proportional to the drift limits.

**Table 2.** Damage states and rotational ductility limits of piers considering flexibility-supported bridge

Damage state	Description	Rotational ductility limits	
		Short pier	Tall pier
Almost none	First yield	1.00	1.00
Slight	Cracking, spalling	1.15	1.13
Moderate	Loss of anchorage	1.59	1.53
Extensive	Incipient pier collapse	2.33	2.19
Complete	Pier collapse	3.07	2.85

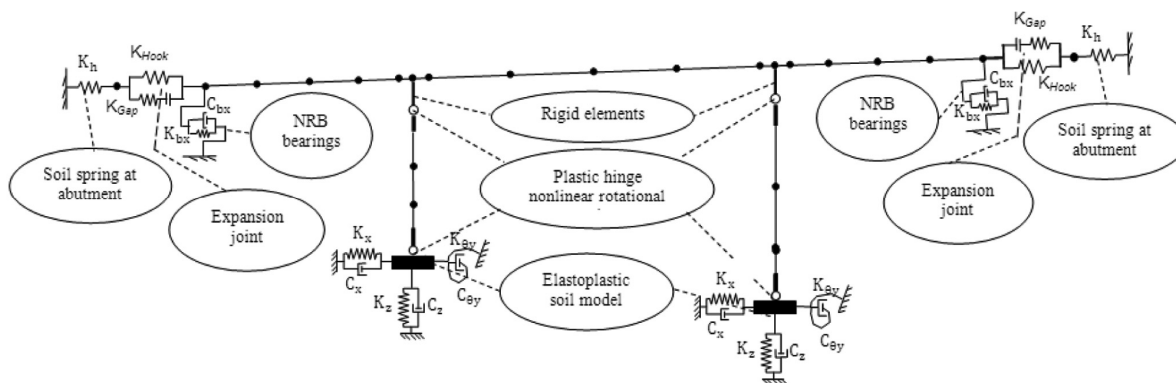


**Figure 4.** Analytical model of the highway bridge under study.

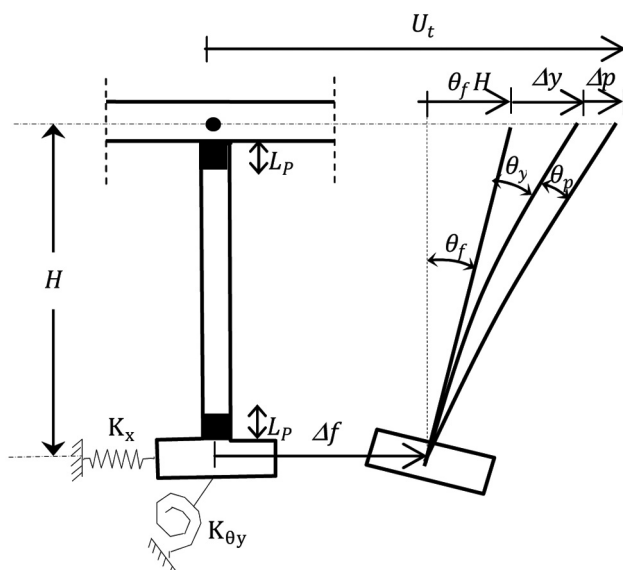


**Figure 5.** A simple soil-structure system representation.

Table 2 illustrates these five damage states and the computed ductility limits in the plastic zones formed at the pier ends of the study bridge in the longitudinal direction.

**Numerical results and discussion**

In order to highlight the bridge progressive failure mechanism, the longitudinal dynamic responses of the

highway bridge, including the effect of abutment stiffness were analysed.

The longitudinal time-history response of temporal variations of rotational ductility demands at pier ends and axial force in the restrainers at the interface of the deck and abutment back wall of the study bridge with backfill soil at the abutments have been evaluated and compared to those of bridge without backfill at the abutments. Newmark direct time-integration method with parameters  $\alpha = 0.5$  and  $\beta = 0.25$  (unconditionally stable average acceleration method) as implemented in SAP2000 (ref. 13) using nonlinear link elements, has been applied to the coupled bridge–foundation system subject to the simulated acceleration input time-history. Details on simulation techniques for the generation of spectrum compatible earthquake motions can be found for example in reference<sup>18</sup>.

*Effects of abutment backfill soil stiffness on rotational ductility demands at pier ends of the bridge*

Figure 6 shows the temporal variations in longitudinal direction of rotational ductility demands at pier ends under simulated earthquake motions. It can be noted from Figure 6a that rotational ductility demands at the bottom of the short pier are more important when effects of abutment backfill soil are ignored leading to the formation of plastic hinge at  $t = 7.29$  s (i.e. when rotational ductility demands at the bottom of the short pier cross the

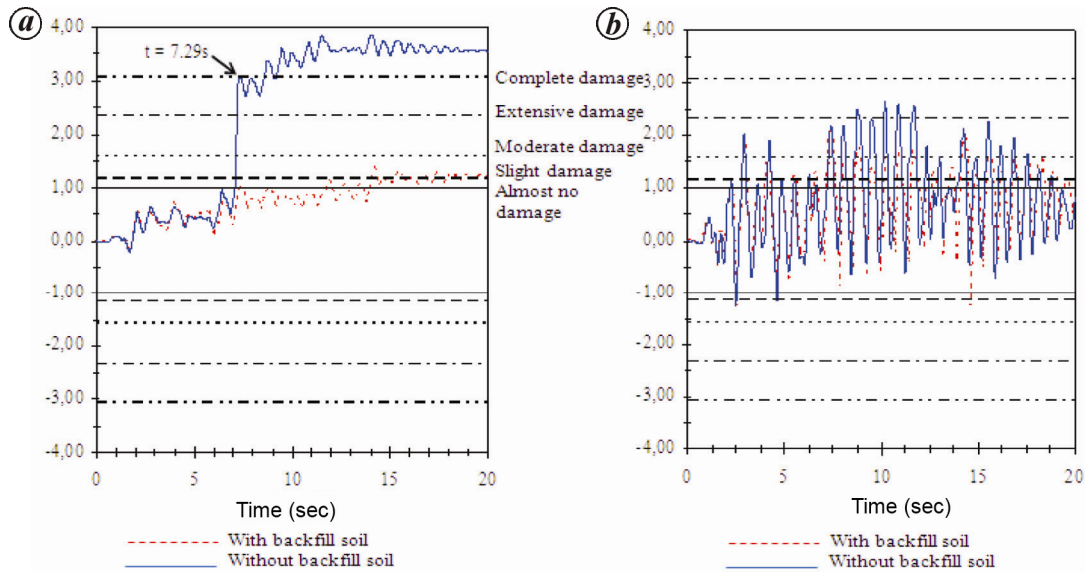


**Figure 6.** Rotational ductility demands in longitudinal direction at pier ends of flexibly-supported bridge model under simulated earthquake motion. *a*, Rotational ductility at the bottom of the short pier. *b*, Rotational ductility at the top of the short pier.

**Table 3.** Maximum ductility demand of plastic hinge and corresponding damage state at column ends of the bridge

		Without backfill		With backfill	
Short pier	Bottom	3.86	Collapse	1.38	Slight to moderate
	Top	2.66	Collapse	2.13	Extensive
High pier	Bottom	0.36	Almost none	0.13	Almost none
	Top	1.79	Moderate	1.11	Slight

pier collapse damage state corresponding to rotational ductility limit value of 3.07). On the other hand, it can be clearly seen from Figure 6a that there is only slight damage when ABSI is considered due to beneficial effect of yielding of abutment backfill soil. The same trends are observed for rotational ductility demands at the top of the short pier. It may therefore be concluded that the bridge failure mechanism can be delayed due to the beneficial effect of ABSI.

Similar conclusions can be drawn for the taller pier. However, ABSI effects are found to be less significant than in the case of the short pier due to higher flexibility of the tall pier (Figure 6b).

#### *Effects of abutment backfill soil on relative displacements and maximal forces at expansion joints*

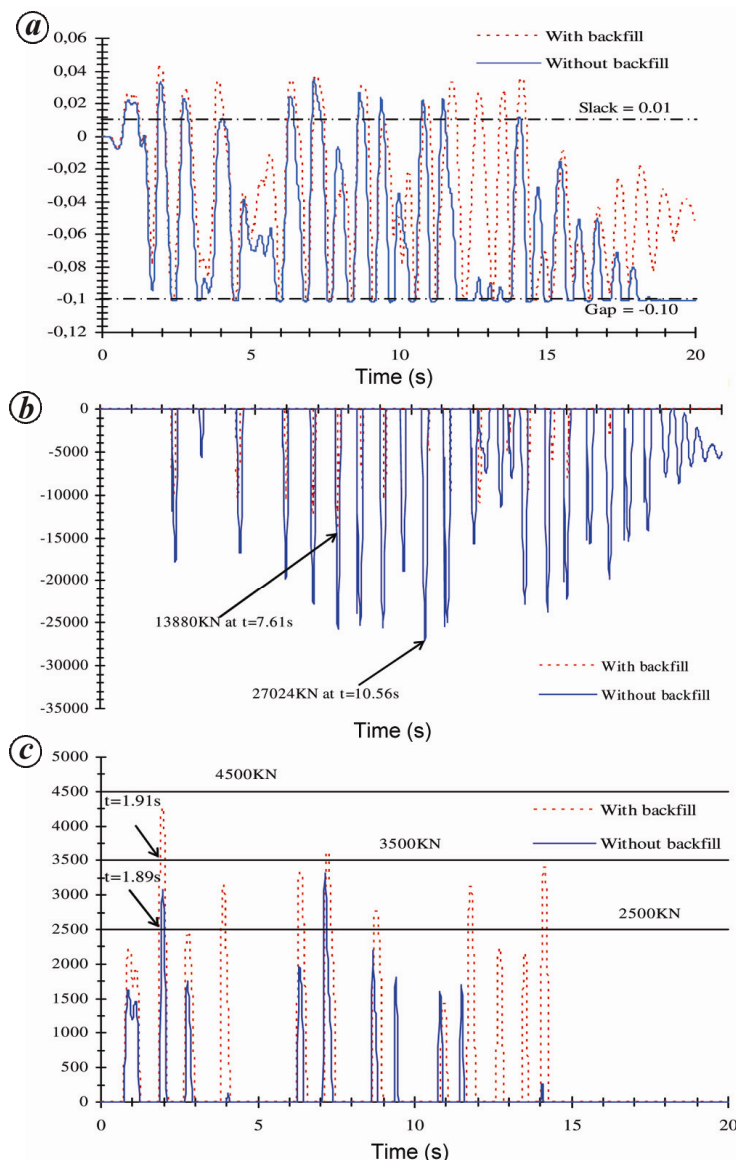
Figure 7a is a plot of the relative displacement time-history at the two ends of the expansion joints. Impact force develops at the bridge deck and abutment back wall when the initial gap is exhausted resulting in pounding.

Figure 7b shows that pounding force is generated only at those time instants when relative inward movement between deck and abutments exceeds the initial gap (0.10 m). It is seen that a maximum impact force of 13,880 kN develops at  $t = 7.61$  sec while including backfill soil effects at abutments, while it becomes to 27,024 kN at  $t = 10.56$  sec (a significant increase of more than 94%) when the backfill soil effects are ignored.

Figure 7c shows time-varying axial force in the restrainers, transmitted to the abutment back walls through anchors devices. It should be noted that the bridge failure mechanism is modified as the design capacity of the restrainers is exceeded. As an example, if the restrainer is assigned to a design capacity of 2500 kN or less, collapse of the bridge occurs due to failure of the restrainer or anchorage at time  $t = 1.89$  sec, regardless of the ABSI effects.

This scenario changes for a different value of design capacity of the restrainers.

For design capacity of the restrainers equal to 3500 kN, the bridge collapses again due to failure of restrainer or anchorage at time  $t = 1.91$  sec when the backfill soil effects are included at the abutments, resulting in



**Figure 7.** *a*, Relative displacement at element pounding. *b*, Pounding force developed at expansion joint. *c*, Axial force in the restrainer.

unseating failure and subsequent bridge collapse of (i.e. deck fall-off).

However, for restrainer capacity of 4500 kN or more, failure cannot occur but plastic hinges form at  $t = 7.29$  sec at the bottom of the short pier and  $t = 9$  sec at the top of the short pier of the bridge, resulting in anticipated bridge collapse.

It also may be concluded that special attention should be given to axial forces in the restrainers whose displacements can be, under certain design conditions, increased due to yielding of the backfill soil.

In order to prevent deck unseating resulting from restrainer failure and subsequent bridge collapse, particular attention should also be given to the proper design of nonlinear characteristics of restrainers and bearing devices.

Table 3 shows maximum ductility demands of plastic hinges and corresponding damage state at column ends for the bottom and top piers of the bridge with and without backfill. It can be noticed from the table that maximal ductility demand responses with and without backfill are significantly different and more importantly, at the bottom of the short pier. In all cases, ABSI can effectively reduce seismic demands of the studied bridge.

### Summary and conclusion

In this study, the influence of ABSI on longitudinal progressive seismic failure and hence identification of the anticipated overall failure mechanism of a highway

bridge with expansion joints at seat-type abutments are presented. FE modelling of the bridge is performed and comparative assessments of the nonlinear seismic response of the bridge when accounting for or neglecting the resistance of the abutments are carried out under simulated earthquake strong ground motions. Bridge responses, including effects of ABSI are discussed in terms of temporal variations of rotational ductility demands at the pier ends, axial forces in the restrainers and pounding forces at the interface of deck and abutment back walls.

From the numerical results obtained in this study, the following main conclusions can be drawn:

- Moment–rotation relationships, including SSI for plastic zones at the pier ends of reinforced concrete bridge and associated rotational ductility limits consistent with five damage states, ranging from yield to collapse, have been established.
- The results obtained clearly demonstrate that ABSI has a significant effect on the seismic response in longitudinal direction and reduces effectively the seismic demand of the studied bridge. In particular, forces at the expansion joints and rotational ductility demands at the pier ends of the bridge (although to a lesser degree for the tallest piers) are reduced by ABSI. However, special attention should be given to axial forces in the restrainers whose displacements can be, under certain design conditions, increased due to yielding of backfill soil.
- In order to prevent deck unseating resulting from restrainer failure and subsequent bridge collapse, particular attention should also be given to proper design of nonlinear characteristics of the restrainers.
- Safer and more economical bridge designs can be obtained by properly accounting for ABSI.

---

1. Wilson, P. and Elgamal, A., Full-scale bridge abutment passive earth pressure experimentation and simulation. *J. Geotech Geoenviron. Eng. (ASCE)*, 2010, **136**, 1634–1643.
2. Ouanani, M. and Tiliouine, B., Effects of foundation soil stiffness on the 3-D modal characteristics and seismic response of a highway bridge. *J. Civ. Eng. (KSCE)*, 2015, **19**(4), 1009–1023.
3. Pecker, A., Influence of nonlinear soil structure interaction on the seismic demand of bridges. In Proceedings of the International Conference on Innovations on Bridges and Soil Bridge Interaction, Athens, Greece, 2011.

4. Kotsoglu, A. and Pantazopoulou, S., Modeling of embankment flexibility and soil-structure interaction in integral bridges. In Proceedings of First European Conference on Earthquake Engineering and Seismology, Geneva, Switzerland, 2006.
5. Mylonakis, G., Gazetas, G., Nikolaou, A. and Michaelides, O., The role of soil on the collapse of 18 piers of the Hanshin Expressway in the Kobe earthquake. In Proceedings of the 12th WCEE, Auckland, New Zealand, 2000.
6. Mitoulis, S. A., Seismic design of bridges with the participation of seat-type abutments. *Eng. Struct.*, 2012, **44**, 222–233.
7. FEMA-356, Prestandard and commentary for seismic rehabilitation of buildings, Federal Emergency Management Agency, Washington DC, USA, 2000.
8. RPOA, Partie I: Ponts, Règles Parasismiques Applicables au Domaine des Ouvrages d'Arts, Algeria, 2008.
9. Gazetas, G., Foundation vibrations. In *Foundation Engineering Handbook* (ed. Fang, H.-Y.) Van Nostrand Reinhold, New York, USA, 1991.
10. FHWA, Seismic design of highway bridge foundations, design procedures and guidelines, Federal Highway Administration, US Department of Transportation, No. RD-94-052, Washington, DC, USA, 1995.
11. Saadeghvaziri, M. A. and Yazdani-Motlagh, A. R., Seismic behavior and capacity demand analyses of three multi-span simply supported bridges. *Eng. Struct.*, 2007, **30**, 54–66.
12. Yoshida, N., Estimation of mechanical soil properties. In *Seismic Ground Response Analysis, Geotechnical, Geological and Earthquake Engineering*, Tokyo Gakuin University, Miyagi, Japan, 2015.
13. Computer and Structures, Inc. SAP2000 (Nonlinear version 15), Nonlinear User's Manual Reference, Berkeley, CA, USA, 2012.
14. Priestley, M. J. N., Calvi, G. M. and Kowalsky, M. J., *Displacement-based Seismic Design of Structures*, IUSS Press, Pavia, Italy, 2007.
15. Mylonakis, G. and Gazetas, G., Seismic soil–structure interaction: beneficial or detrimental? *J. Earthquake Eng.*, 2011, **4**, 121–138.
16. Sextos, A., Pitilakis, K. and Kappos, A., Inelastic dynamic analysis of RC bridges accounting for spatial variability of ground motion, site effects and soil–structure interaction phenomena. Part A: methodology and analytical tools. *Earthquake Engineering and Structural Dynamics*, 2003, **4**, 607–629.
17. Dutta, A. and Mander, J. B., Seismic fragility analysis of highway bridges. In Proceedings of the Center-to-Center Project Workshop on Earthquake Engineering Frontiers in Transportation Systems, Tokyo, Japan, 1999.
18. Tiliouine, B., Hammoutene, M. and Bard, P. Y., Phase angle properties of earthquake strong motions: a critical look. In Proceedings of the 12th World Conference on Earthquake Engineering, Auckland, New Zealand, 2000.

Received 2 January 2016; revised accepted 31 August 2016

doi: 10.18520/cs/v112/i02/355-363